MNRAS **000**, 1–5 (2016) Preprint 21 September 2016 Compiled using MNRAS LATEX style file v3.0

On the surface physics affecting solar oscillation frequencies

G. Houdek,[1⋆] R. Trampedach,[2,1] M. J. Aarslev,[1] J. Christensen-Dalsgaard[1]
[1] *Stellar Astrophysics Centre, Department of Physics and Astronomy, Aarhus University, 8000 Aarhus C, Denmark*
[2] *Space Science Institute, 4750 Walnut Street, Suite 205, Boulder, CO 80301, USA*

arXiv:1609.06129v1 [astro-ph.SR] 20 Sep 2016

Accepted XXX. Received YYY; in original form ZZZ

ABSTRACT
Adiabatic oscillation frequencies of stellar models, computed with the standard mixing-length formulation for convection, increasingly deviate with radial order from observations in solar-like stars. Standard solar models overestimate adiabatic frequencies by as much as $\sim 20\mu$Hz. In this letter, we address the physical processes of turbulent convection that are predominantly responsible for the frequency differences between standard models and observations, also called 'surface effects'. We compare measured solar frequencies from the MDI instrument on the SOHO spacecraft with frequency calculations that include three-dimensional (3D) hydrodynamical simulation results in the equilibrium model, nonadiabatic effects, and a consistent treatment of the turbulent pressure in both the equilibrium and stability computations. With the consistent inclusion of the above physics in our model computation we are able to reproduce the observed solar frequencies to $\lesssim 3\mu$Hz without the need of any additional ad-hoc functional corrections.

Key words: Sun: oscillations – convection – hydrodynamics – turbulence

1 INTRODUCTION

High-quality measurements of stellar oscillation frequencies of thousands of solar-like stars are now available from the NASA space mission *Kepler*, and from the French satellite mission CoRoT (Convection Rotation and planetary Transits). In order to exploit these data for probing stellar interiors, accurate modelling of stellar oscillations is required. However, adiabatically computed frequencies are increasingly overestimated with increasing radial order (see dot-dashed curve in Fig. 1). These effects have become known as 'surface effects' (e.g., Brown 1984; Gough 1984; Balmforth 1992b; Rosenthal et al. 1999; Houdek 2010; Grigahcène et al. 2012). Semi-empirical corrections to adiabatically computed frequencies proposed by e.g., Kjeldsen et al. (2008), Ball & Gizon (2014), Sonoi et al. (2015), Ball et al. (2016) are purely descriptive and provide little physical insight. Here, we report on a self-consistent model computation, which reproduces the observed solar frequencies to within $\sim 3\mu$Hz, and, for the first time, without the need of any ad-hoc functional corrections. It represents a purely physical explanation for the 'surface effects' by considering (a) a state-of-the-art 3D–1D patched mean model, (b) nonadiabatic effects, (c) a consistent treatment of turbulent pressure in the mean and pulsation models, and (d) a depth-dependent modelling of the turbulent anisotropy in both the mean and oscillation calculations.

Convection modifies pulsation properties of stars principally through three effects:

(i) effects through the turbulent pressure term in the hydrostatic equation (structural effect), and its pulsational perturbation in the momentum equation (modal effect);
(ii) opacity variations brought about by large convective temperature fluctuations, affecting the mean stratification; this structural effect is also known as 'convective backwarming' (e.g., Trampedach et al. 2013);
(iii) nonadiabatic effects, additional to the pulsational perturbed radiative heat flux, through the perturbed convective heat flux (modal effects) in the thermal energy equation.

We follow Rosenthal et al.'s (1999) idea of replacing the outer layers of a 1D solar envelope model by an averaged 3D simulation, and adopt the most advanced and accurate 3D – 1D matching procedure available today (Trampedach et al. 2014a,b) for estimating structural effects on adiabatic solar frequencies. Furthermore, we use a 1D nonlocal, time-dependent convection model for estimating the modal effects of nonadiabaticity and convection dynamics.

Additional modal effects can be associated with the advection of the oscillations by spatially varying turbulent flows in the limit of temporal stationarity (Brown 1984; Zhugzhda & Stix 1994; Bhattacharya et al. 2015). This 'advection picture' is related to the 'dynamical picture' of including temporally varying turbulent convection fluctuations in the limit of spatially horizontal homogeneity. Because these two pictures describe basically the same effect

⋆ E-mail: hg@phys.au.dk

© 2016 The Authors

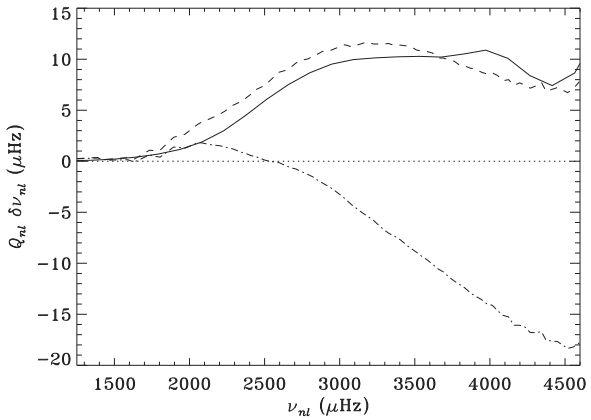

Figure 1. Inertia-scaled frequency differences between MDI measurements (Sun) of acoustic modes with degree $l = 20$–23 and model computations as functions of oscillation frequency. The scaling factor Q_{nl} for a mode with radial order n, is obtained from taking ratios between the inertia of modes with $l = 23$ and radial modes, interpolated to the $l = 23$ frequencies (e.g., Aerts et al. 2010). The dot-dashed curve shows the differences for baseline model, 'Sun - A' (cf. Section 2.2.2), reflecting the results for a standard solar model computation. The dashed curve plots the residuals for the patched model which includes turbulent pressure and convective back-warming in the mean model, i.e. 'Sun - B (cf. Section 2.2.3)'. The solid curve illustrates the differences from the modal effects of nonadiabaticity and perturbation to the turbulent pressure, i.e. 'D - C' (cf. Section 2.2.4).

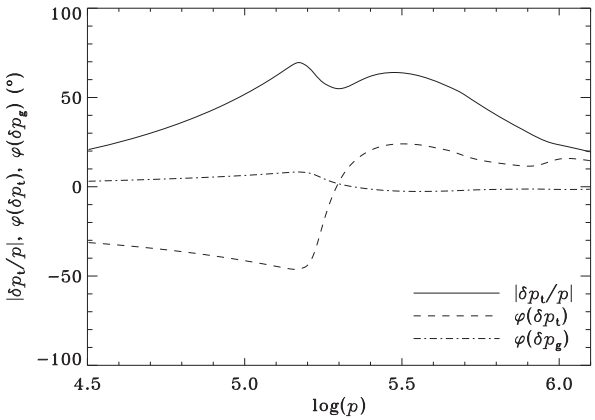

Figure 2. Norm of the relative turbulent pressure eigenfunction $|\delta p_t/p|$ (solid curve) and phases of δp_t (dashed curve) and gas pressure perturbations δp_g (dot-dashed curve); the relative displacement eigenfunction is normalized to unity at the surface. Results are shown for a radial mode with frequency $\nu \simeq 2947\ \mu$Hz, obtained with the solar envelope model 'D' of Section 2.2.4.

but in two different limits, i.e. they are complementary, only one of them should be included. We do so by adopting the latter.

2 MODEL COMPUTATIONS

We use stellar envelope models in which the total pressure $p = p_g + p_t$ satisfies the equation for hydrostatic support,

$$\frac{dp}{dm} = -\frac{1}{4\pi r^2}\frac{Gm}{r^2}\,, \tag{1}$$

where p_g is the gas pressure and p_t the turbulent pressure, $p_t := \overline{\rho w w}$, with w being the vertical component of the convective velocity field $\boldsymbol{u} = (u, v, w)$, and an overbar indicates an ensemble average. The other symbols are mass m, radius r, mass density ρ, and gravitational constant G.

2.1 Adiabatic pulsations of mean models constructed with turbulent pressure

If turbulent pressure is included in the model's mean stratification, particular care must be given to frequency calculations that neglect the pulsational perturbation to the turbulent pressure. In an adiabatic treatment the relative gas pressure perturbation $\delta p_g/p_g$ is related to the relative density perturbation $\delta\rho/\rho$ by the linearized expression

$$\frac{\delta\rho}{\rho} = \frac{1}{\gamma_1}\frac{\delta p_g}{p_g} = \frac{1}{\gamma_1}\frac{p}{p_g}\left(\frac{\delta p}{p} - \frac{\delta p_t}{p}\right)\,, \tag{2}$$

where $\delta X(m)$ are perturbations following the motion, and $\gamma_1 := (\partial \ln p_g/\partial \ln \rho)_s$ is the first adiabatic exponent with s being specific entropy. A standard adiabatic calculation typically neglects convection dynamics, i.e. the effect of the perturbation to the turbulent pressure, $\delta p_t/p$, leading to the approximate linearized expression for an adiabatic change

$$\frac{\delta\rho}{\rho} \simeq \frac{1}{\gamma_1}\frac{p}{p_g}\frac{\delta p}{p}\,. \tag{3}$$

Neglecting δp_t in the full expression (2) for an adiabatic change is partially justified from full nonadiabatic pulsation calculations, in which the turbulent pressure and its pulsational perturbation, δp_t, are consistently included. Such a pulsation computation, in which the pulsational perturbation to the convective heat flux and turbulent pressure is obtained from a time-dependent convection model (e.g., Houdek & Dupret 2015), shows that δp_t varies predominantly in quadrature with perturbation δp_g. This is illustrated in Fig. 2, for the 1D solar envelope model computed according to Section 2.2.4, where the phases $\varphi(\delta p_t)$ (dashed curve) and $\varphi(\delta p_g)$ (dot-dashed curve) of turbulent and gas pressure perturbations are plotted as a function of the total pressure p for a particular radial mode. The solid curve is the norm $|\delta p_t/p|$ of the relative turbulent pressure eigenfunction. In layers where $|\delta p_t/p|$ is largest, the difference between $\varphi(\delta p_t)$ and $\varphi(\delta p_g)$ can be as large as $\sim 60^\circ$, indicating that the turbulent pressure perturbation contributes predominantly to the imaginary part of the complex eigenfrequency, i.e. to the damping or driving of the pulsation modes.

Equation (3) describes consistently, in view of the p_t-term in the hydrostatic equation (1), the approximation of neglecting δp_t in the adiabatic frequency calculations. Therefore, if turbulent pressure is included in the stellar equilibrium structure, the only modification to the adiabatic oscillation equations is the inclusion of the factor p/p_g in the expression for an adiabatic change (3) (see also Rosenthal et al. 1999). Omitting this factor is inconsistent with neglecting δp_t in the adiabatic frequency calculations.

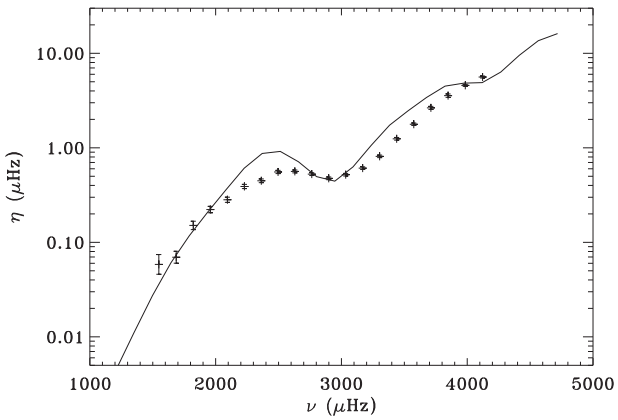

Figure 3. Radial damping rates in units of cyclic frequency of model 'D' (values are connected by solid lines) are compared with BiSON measurements of half the linewidths in the spectral peaks of the observed solar power spectrum (symbols with error bars; from Chaplin et al. 2005).

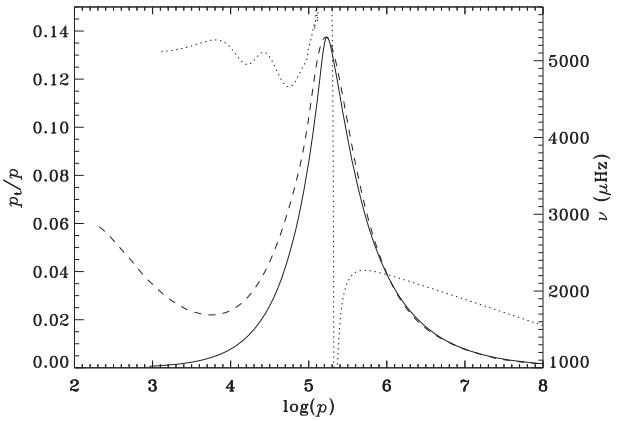

Figure 4. Comparison of the turbulent pressure over total pressure between the patched mean model 'B' (dashed curve), for which the convection zone was modelled by averaged 3D simulation results, and the calibrated nonlocal mean model 'D' (solid curve), as functions of the logarithmic total pressure. The dotted curve is the acoustic cutoff frequency (e.g., Aerts et al. 2010) indicating the region of mode propagation ($\log p \gtrsim 5.3$).

2.2 Envelope models

The convection effects on the mean model structure are investigated by comparing envelope models, computed with either the standard mixing-length formulation or by adopting appropriately averaged 3D simulation results for the outer layers of the convective envelope, with solar frequencies measured by the MDI[1] instrument (Scherrer et al. 1995) on the SOHO[2] spacecraft. The modal effects are estimated by comparing adiabatic and nonadiabatic frequencies from 1D envelope models constructed with a nonlocal, time-dependent formulation for the mean and pulsational perturbations to the convective heat flux and turbulent pressure.

The adopted models are

A: adiabatically computed oscillations of a 1D baseline model constructed with the standard mixing-length formulation (Böhm-Vitense 1958) for convection.

B: adiabatically computed oscillations of a patched model that was constructed by replacing the outer parts of the convection zone of the baseline model, BM, by averaged hydrodynamical simulation results. It therefore includes the turbulent pressure and the effect of convective back-warming in the mean model. The turbulent pressure perturbation, $\delta p_{\rm t}$, is omitted in the adiabatic oscillation calculations according to equation (3).

C: adiabatically computed oscillations of a 1D nonlocal mixing-length model including turbulent pressure $p_{\rm t}$ in the equation of hydrostatic support, but omitting convective back-warming and the effect of the pulsational Lagrangian perturbations to the turbulent pressure in the adiabatic oscillation calculations according to equation (3).

D: nonadiabatically computed oscillations of the same 1D nonlocal mean model used for model 'C', including the Lagrangian perturbations to turbulent pressure, $\delta p_{\rm t}$, and to the convective heat flux.

[1] Michelson Doppler Imager
[2] SOlar and Heliospheric Observatory

2.2.1 The 3D convective atmosphere simulation

The 3D simulation, described by Trampedach et al. (2013), evolves the conservation equations of mass, momentum and energy on a regular grid, which is optimized in the vertical direction to capture the photospheric transition. The equation of state (EOS) is a custom calculation of Mihalas et al.'s (1988) EOS for the employed 15 element mixture, and the monochromatic opacities are described by Trampedach et al. (2014a). Radiative transfer is solved explicitly with the hydrodynamics, and line-blanketing (non-greyness) is accounted for by a binning of the monochromatic opacities, as developed by Nordlund (1982). The top and bottom boundaries are open and transmitting, minimizing their effect on the interior of the simulation. The constant entropy assigned to the inflows at the bottom is adjusted to obtain the solar effective temperature $T_{\rm eff}$.

2.2.2 Baseline model - 'A'

The baseline model is a 1D solar envelope model integrated from a Rosseland optical depth of $\tau = 10^{-4}$ down to a depth of 5% $R_\odot$, and using Böhm-Vitense's (1958) mixing-length formulation for convection. The model is computed with a code (Christensen-Dalsgaard & Frandsen 1983) that is closely related to Christensen-Dalsgaard's (2008) stellar evolution code ASTEC. The turbulent pressure is omitted in the hydrostatic equation (1). The 1D model adopts the same atomic physics as the 3D atmosphere simulation described above in Section 2.2.1. The 3D simulation also provides the temperature-optical-depth relation and the mixing length for the 1D baseline model (Trampedach et al. 2014a,b). This is accomplished by matching the 1D baseline model to the 3D simulation at a common pressure sufficiently deep that the 3D convective fluctuations can be considered linear and far enough from the bottom of the 3D spatial domain that boundary effects are negligible. The total mass and luminosity are identical for the 1D baseline model and the 3D

simulation, whereas $T_{\rm eff}$ and surface gravity are diluted in the latter case by the convective expansion of the 3D atmosphere, which also gives rise to the stratification part of the 'surface effects' in the patched model of Section 2.2.3. The limited extent of the envelope models restricts our mode selection to those that have lower turning points well inside the lower boundary. Choosing modes with degree $l = 20$–23 fulfils this requirement, as well as ensures that the modes are predominantly radial on the scale of the thin layer giving rise to the surface effects.

2.2.3 Patched model with $p_{\rm t}$ - 'B'

Since the 1D baseline model is matched continuously to the 3D simulation (see Section 2.2.2), the two solutions can be combined to a single, patched, model for the adiabatic oscillation calculations. This, however, demands one more step: the 3D simulation is carried out in the plane-parallel approximation, and their constant gravitational acceleration introduces significant glitches in some quantities. We therefore apply a correction for sphericity, consistent with the radius of the 1D model.

2.2.4 Nonlocal models with $p_{\rm t}$ - 'C & D'

The 1D nonlocal model calculations with turbulent pressure are carried out essentially in the manner described by Houdek et al. (1999, see also Balmforth 1992a). The convective heat flux and turbulent pressure are obtained from a nonlocal generalization of the mixing-length formulation (Gough 1977b,a). In this generalization three more parameters, a, b and c, are introduced which control the spatial coherence of the ensemble of eddies contributing to the total convective heat flux (a) and turbulent pressure (c), and the degree to which the turbulent fluxes are coupled to the local stratification (b). The effects of varying these nonlocal parameters on the solar structure and oscillation properties were discussed in detail by Balmforth (1992a).

The nonlocal parameter c is calibrated such as to have the maximum value of the turbulent pressure, $\max(p_{\rm t})$, in the 1D nonlocal model to agree with the 3D simulation result (see Fig. 4). The depth-dependence of the anisotropy $\Phi := \boldsymbol{u} \cdot \boldsymbol{u}/w^2$ of the convective velocity field is adapted from the 3D simulations using an analytical function with the maximum 3D value in the atmospheric layers and the minimum 3D value in the deep interior of the simulations. The remaining nonlocal parameters a and b cannot be easily obtained from the 3D simulations and are therefore calibrated such as to have a good agreement between calculated damping rates and measured solar linewidths (see Fig. 3). The mixing length was calibrated to the helioseismically determined convection-zone depth $d_{\rm cz}/{\rm R}_\odot \simeq 0.287$ (Christensen-Dalsgaard et al. 1991). Both the envelope and pulsation calculations assume the generalized Eddington approximation to radiative transfer (Unno & Spiegel 1966). The abundances by mass of hydrogen and heavy elements are adopted from the patched model 'B', i.e. $X = 0.736945$ and $Z = 0.018055$. The opacities are obtained from the OPAL tables (Iglesias & Rogers 1996), supplemented at low temperature by tables from Kurucz (1991). The EOS includes a detailed treatment of the ionization of C, N, and O, and a treatment of the first ionization of the next seven most abundant elements (Christensen-Dalsgaard 1982). The integration of stellar-structure equations starts at an optical depth of $\tau = 10^{-4}$ and ends at a radius fraction $r/{\rm R}_\odot = 0.2$. The temperature gradient in the plane-parallel atmosphere is corrected by using a radially varying Eddington factor fitted to Model C of Vernazza et al. (1981).

The linear nonadiabatic pulsation calculations are carried out using the same nonlocal convection formulation with the assumption that all eddies in the cascade respond to the pulsation in phase with the dominant large eddies. A simple thermal outer boundary condition is adopted at the temperature minimum where for the mechanical boundary condition the solutions are matched smoothly onto those of a plane-parallel isothermal atmosphere (e.g., Balmforth et al. 2001). At the base of the model envelope the conditions of adiabaticity and vanishing of the displacement eigenfunction are imposed. Only radial p modes are considered.

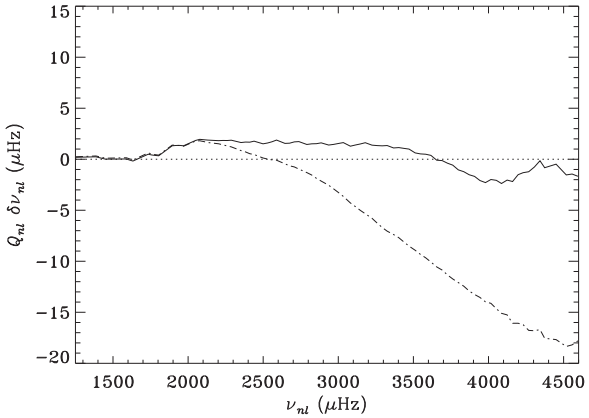

Figure 5. Inertia-scaled frequency difference between MDI data (Sun) and model calculations. The solid curve includes the combined frequency corrections arising from structural effects ('B') and modal effects ('D'). The dot-dashed curve is the result for our baseline model 'A', reflecting the result for a 'standard' solar model computation.

3 RESULTS AND DISCUSSION

The adiabatic frequency corrections (Section 2.1) arising from modifications to the stratification of the mean model are obtained from an appropriately averaged 3D simulation for the outer convection layers (Section 2.2.3).

The frequency corrections associated with modal effects arising from nonadiabaticity, including both the perturbations to the radiation and convective heat flux, and from convection-dynamical effects of the perturbation to the turbulent pressure, are estimated from a 1D nonlocal, time-dependent convection model including turbulent pressure (Section 2.2.4).

3.1 Adiabatic frequency corrections from modifications to the mean structure

Frequency differences between MDI data (Sun) and our baseline model, 'Sun - A', are depicted in Fig. 1 by the dot-

dashed curve, illustrating the well-known 'surface effects' for a standard solar model with a frequency residual up to $\sim 20\,\mu$Hz. The effect on the adiabatic frequencies by adopting an averaged 3D simulation for the outer convection layers is illustrated by the dashed curve in Fig. 1. It shows the frequency difference between MDI data and the patched model, 'Sun - B'. The patched model underestimates the frequencies by as much as $\sim 10\,\mu$Hz. The change from overestimating the frequencies with the baseline model, 'A' (dot-dashed curve), to underestimating the frequencies with the patched model, 'B' (dashed curve), is mainly due to effects of turbulent pressure $p_{\rm t}$ in the equation of hydrostatic support (1) and from opacity changes (convective back-warming) of the relatively large convective temperature fluctuations in the superadiabatic boundary layers.

3.2 Modal effects from nonadiabaticity and convection dynamics

Additional to the structural changes we also consider the modal effects of nonadiabaticity and pulsational perturbation to turbulent pressure $\delta p_{\rm t}$. We do this by using the 1D solar envelope model of Section 2.2.4, which includes turbulent pressure, and which is calibrated such as to have the same $\max(p_{\rm t})$ as the 3D solar simulation (see Fig. 4). To assess the modal effects we compute for this nonlocal envelope model nonadiabatic and adiabatic frequencies. The frequency differences between these two model computations, i.e. 'D - C', is plotted in Fig. 1 with a solid curve, and illustrates the modal effects of nonadiabaticity and turbulent pressure perturbations $\delta p_{\rm t}$. These modal effects (solid curve in Fig. 1) produce frequency residuals that are similar in magnitude to the frequency residuals between the Sun and the patched model, 'Sun - B' (dashed curve). This suggests that the underestimation of the adiabatic frequencies due to changes in the mean model, 'B', is nearly compensated by the modal effects. The remaining overall frequency difference between the Sun and models that include both structural and modal effects, i.e. the difference between the dashed and solid curves in Fig. 1, is illustrated in Fig. 5 by the solid curve, showing a maximum frequency difference of $\sim 3\,\mu$Hz. Also depicted, for comparison, is the dot-dashed curve from Fig. 1, which shows the frequency difference for the baseline model 'A', representing the result for a standard solar model calculation.

We conclude that, if both structural and modal effects due to convection and nonadiabaticity are considered together, it is possible to reproduce the measured solar frequencies satisfactorily (solid curve in Fig. 5) without the need of any ad-hoc correction functions. Moreover, the calibrated set of convection parameters in the 1D nonlocal model calculations reproduces the turbulent-pressure profile of the 3D simulation in the relevant wave-propagating layers (Fig. 4), the correct depth of the convection zone, and solar linewidths over the whole measured frequency range (Fig. 3). Although we have not used the same equilibrium model for estimating the structural ('B') and the modal effects ('D'), we believe that this remaining inconsistency is minute on the estimated modal effects, because of the satisfactory reproduction of the $p_{\rm t}$ profile in the nonlocal equilibrium model 'D' (see Fig. 4). However, we do plan to address this in a future paper.

ACKNOWLEDGEMENTS

We thank Douglas Gough for many inspiring discussions. RT acknowledges funding from NASA grant NNX15AB24G. Funding for the Stellar Astrophysics Centre is provided by The Danish National Research Foundation (Grant DNRF106).

REFERENCES

Aerts C., Christensen-Dalsgaard J., Kurtz D., 2010, Asteroseismology. Springer
Ball W. H., Gizon L., 2014, A&A 568, A123
Ball W. H., Beeck B., Cameron R. H., Gizon L., 2016, A&A 592, A159
Balmforth N. J., 1992a, MNRAS 255, 603
Balmforth N. J., 1992b, MNRAS 255, 632
Balmforth N. J., Cunha M. S., Dolez N., Gough D. O., Vauclair S., 2001, MNRAS 323, 362
Bhattacharya J., Hanasoge S., Antia H. M., 2015, ApJ 806, 246
Böhm-Vitense E., 1958, Zeitschrift für Astrophysik 46, 108
Brown T. M., 1984, Science 226, 687
Chaplin W. J., Houdek G., Elsworth Y., Gough D. O., Isaak G. R., New R., 2005, MNRAS 360, 859
Christensen-Dalsgaard J., 1982, MNRAS 199, 735
Christensen-Dalsgaard J., 2008, Ap&SS 316, 13
Christensen-Dalsgaard J., Frandsen S., 1983, Sol. Phys. 82, 469
Christensen-Dalsgaard J., Gough D. O., Thompson M. J., 1991, ApJ 378, 413
Gough D. O., 1977a, in Spiegel E. A., Zahn J.-P., eds, Lecture Notes in Physics Vol. 71, Problems of Stellar Convection. Springer, Heidelberg, pp 15–56
Gough D. O., 1977b, ApJ 214, 196
Gough D. O., 1984, Advances in Space Research 4, 85
Grigahcène A., Dupret M.-A., Sousa S. G., Monteiro M. J. P. F. G., Garrido R., Scuflaire R., Gabriel M., 2012, MNRAS 422, L43
Houdek G., 2010, Astronomische Nachrichten 331, 998
Houdek G., Dupret M.-A., 2015, Living Rev. in Solar Phys. 12
Houdek G., Balmforth N. J., Christensen-Dalsgaard J., Gough D. O., 1999, A&A 351, 582
Iglesias C. A., Rogers F. J., 1996, ApJ 464, 943
Kjeldsen H., Bedding T. R., Christensen-Dalsgaard J., 2008, ApJ 683, L175
Kurucz R. L., 1991, in Crivellari L., Hubeny I., Hummer D. G., eds, NATO Series C Vol. 341, NATO (ASI). p. 441
Mihalas D., Dappen W., Hummer D. G., 1988, ApJ 331, 815
Nordlund Å., 1982, A&A 107, 1
Rosenthal C. S., Christensen-Dalsgaard J., Nordlund Å., Stein R. F., Trampedach R., 1999, A&A 351, 689
Scherrer P. H., et al., 1995, Sol. Phys. 162, 129
Sonoi T., Samadi R., Belkacem K., Ludwig H.-G., Caffau E., Mosser B., 2015, A&A 583, A112
Trampedach R., Asplund M., Collet R., Nordlund Å., Stein R. F., 2013, ApJ 769, 18
Trampedach R., Stein R. F., Christensen-Dalsgaard J., Nordlund Å., Asplund M., 2014a, MNRAS 442, 805
Trampedach R., Stein R. F., Christensen-Dalsgaard J., Nordlund Å., Asplund M., 2014b, MNRAS 445, 4366
Unno W., Spiegel E. A., 1966, PASJ 18, 85
Vernazza J. E., Avrett E. H., Loeser R., 1981, ApJS 45, 635
Zhugzhda Y. D., Stix M., 1994, A&A 291, 310

This paper has been typeset from a TEX/LATEX file prepared by the author.